Part II

Nucleon-Nucleus and Antinucleon-Nucleus Interactions

Nonrelativistic and Relativistic Treatments of Nucleon-Nucleus Scattering

L. Ray
Department of Physics
The University of Texas at Austin
Austin, Texas 78712 USA

ABSTRACT

Both nonrelativistic and relativistic models for describing nucleon-nucleus scattering from low to intermediate energies are considered. In particular the effect of virtual $\Delta(1232\ \text{MeV})$ and $N^*(1440\ \text{MeV})$ nucleon resonances on the Pauli blocking modification of the low energy nonrelativistic nucleon-nucleon effective interaction is calculated for several partial wave channels. The effects of Pauli blocking at energies above the pion production threshold are also examined. Applications of the relativistic impulse approximation (RIA) - Dirac equation approach to recent 800 MeV proton-nucleus spin rotation data are given. Preliminary estimates of second order multiple scattering contributions arising from two-nucleon correlations in the target nucleus are studied within the context of the RIA model.

I. INTRODUCTION

The nuclear system consisting of a single nucleon interacting with a composite nucleus has, during the last several decades, provided nuclear physicists with a rich and rewarding area of research in which to study and determine nuclear structure properties and to test and evaluate many-body theories. In particular the scattering of protons and neutrons from nuclei via elastic, inelastic, pick-up, knock-out and quasi-free processes has provided a wealth of information including nuclear sizes, collective and single particle excited state structures, spatial and momentum distributions, etc. Ironically, however, the theoretical interpretation of the simplest nucleon-nucleus reaction, namely elastic scattering, remains the subject of debate among theorists concerned with understanding this many-body system in terms of the elementary two-body interaction and target nucleus structure information. Questions concerning the importance of relativity, medium modifications, intermediate nuclear structure (correlation) effects, non-localities, mesonic, quark and isobar degrees of freedom, etc. have been only partially answered. The fact that the nucleon-nucleus system is presently only qualitatively understood is a tribute to the rich, complexity of the nuclear many-body problem.

At present the only available theories of the nucleon-nucleus system which are at all tractable are those derived from the nonrelativistic (NR) many-body

Schrödinger equation (e.g., Brueckner theory,[1] the multiple scattering approaches of Watson[2] and Kerman, McManus and Thaler (KMT),[3] etc.). One of the most successful applications of this approach at low energies can be found in the work of H. V. von Geramb and co-workers[4] in which the 0 - 400 MeV nucleon-nucleus elastic scattering data are quantitatively explained using the Brueckner G-matrix for positive energy (continuum) nucleons as the effective interaction between the projectile nucleon and the bound nucleons inside the target nucleus. In these calculations realistic two-body interactions are assumed; Pauli blocking, Fermi motion averaging, and intermediate binding potential effects are all included. A particular limitation of this model is the omission of internal nucleon degrees of freedom which renders the calculations inapplicable above 350 MeV and could in principle cast doubt on the reliability of the model at low energies where nucleon structure effects could still contribute to the effective two-body interaction by way of virtual processes. This question will be studied in detail in Section II. Here it is shown that nucleon internal structure effects (i.e., virtual isobar excitation) at energies below the two-body inelastic threshold are negligible. Furthermore, it is shown that Pauli blocking corrections are expected to be minimal at energies at and above 500 MeV. These results, together with other works, (see Section III) suggest that the success of NR models in explaining nucleon-nucleus scattering data above 400 MeV is problematic.

In the last few years an important developement in the understanding of nucleon-nucleus physics has been the realization that virtual proton-antiproton pair processes contribute significantly to intermediate energy proton-nucleus (pA) elastic scattering observables, particularly the analyzing power, $A_y(\theta)$, and spin rotation, $Q(\theta)$.[5-8] The basis for this finding is discussed in Section III where the so-called relativistic impulse approximation (RIA) - Dirac equation model of pA elastic scattering is applied to several recent data sets. Although the RIA is not a "theory" it does point the way toward a more fundamental understanding and accurate description of nucleon-nucleus elastic scattering. Some of the latest refinements to the RIA approach are discussed in Section IV with special attention being given to recent estimates of the effects of target nucleon correlations. Finally, a summary and prospectus are given in Section V.

II. NR PAULI BLOCKING EFFECTS BELOW AND ABOVE PION PRODUCTION THRESHOLD

In order to extend the medium modified effective interaction of von Geramb[4] and others[9,10] above the pion production threshold, models of the nucleon-nucleon (NN) interaction which account for NN inelasticity are required. Since most of the NN inelasticity in the intermediate energy range below 1 GeV involves the formation of

the $\Delta(1232\ \text{MeV})$ resonance[11] it is reasonable to use a NN-isobar model to describe NN elastic scattering above 350 MeV. Such a model has been completely developed by Lomon[11] and forms the basis of the calculations presented here. Other intermediate energy NN interaction models have been presented[12-14] and should also be utilized in studies of medium effects above 350 MeV.

The NN scattering model considered here permits NN, nucleon-isobar, and isobar-isobar channels.[11] Non-resonant nucleon-nucleon-pion ($NN\pi$) channels are included in the scalar (two pion exchange) term in the diagonal NN interaction potential.[15] The model is based on the coupled channels NN interaction of Lomon[11] which is an extension of the earlier Feshbach-Lomon (FL) boundary condition model.[15] In the present work the FL interaction for the NN channels and the N-isobar coupling potentials beyond the core radius ($r_c = 0.73469$ fm) are taken from Ref. 11 in each partial wave channel without alteration, as are the coupling schemes. The FL NN interaction beyond the core radius relies on meson exchange models of the interaction where pion, η, ρ, ω and nonresonant 2π exchanges are assumed. This model is particularly suited for this coupled channels isobar calculation since the theoretical FL potential does not include intermediate isobar (resonance) contributions, so that double counting of the isobar effects are readily avoided. The coupling potentials of Lomon beyond r_c are generally taken from one-pion exchange models but also include phenomenological pieces. The elastic scattering channel is fairly insensitive to the isobar-nucleon diagonal interaction; it has therefore been omitted for $r > r_c$ as is done in Ref. 11.

Rather than specifying an empirical boundary condition at r_c as in Ref. 11, a phenomenological, energy independent core potential is generated which, together with the potentials for $r > r_c$ and the couplings, reproduces the NN phase shifts from 0 - 1000 MeV. The core potential, rather than just the boundary condition on the wave function at $r = r_c$, is needed in order to determine the NN wave function inside the core radius, this being required in order to obtain the medium modified NN effective interaction.

The finite widths of the isobars are included in Ref. 11 by explicitly coupling to many discrete excited channels. This straightforward method for accounting for the finite isobar lifetime is numerically very time consuming for the core potential model used here and would be completely impractical for the integral equation, medium effect calculations which follow. Therefore, in the calculations presented here the finite isobar widths have been accounted for by assuming a complex isobar mass as in Ref. 14.

The model employed here can be summarized by the following set of coupled equations,

$$\{\frac{d^2}{dr^2} - \frac{\ell_i(\ell_i+1)}{r^2} + k_i^2\}\phi_i = \frac{2\mu_i}{\hbar^2} \sum_j V_{ij}\ \phi_j \qquad [1a]$$

$$\{\frac{d^2}{dr^2} - \frac{\ell_j(\ell_j+1)}{r^2} + \tilde{k}_j^2\}\phi_j = \frac{2\mu_j}{\hbar^2} \sum_i V_{ji}\ \phi_i . \qquad [1b]$$

In Eq. (1) $i,j = 1,2$ represent NN tensor coupled channels, $i,j = 3,4 \cdots$ represent isobar channels, $\mu_i = m_i^{(1)}m_i^{(2)}/(m_i^{(1)}+m_i^{(2)})$, m_i is the nucleon or isobar mass, k_i is the NN channel wave number, ϕ_i the radial part of the wave function describing the relative two-body motion, and V_{ij} is the potential matrix. The isobar channel momentum is set equal to (Γ = isobar width in MeV)[14]

$$\tilde{k}_j^2 = k_j^2 + i\,\frac{\mu_j}{\hbar^2}\,\Gamma_j \qquad [2]$$

for the N-Δ and N-N^* channels only. The width of the Δ-Δ isobar channel assumed in Ref. 11 is not important for $T_{LAB} \leq 1$ GeV. For complex momentum, the N-isobar channels are matched to asymptotic boundary conditions of the form

$$\phi_{N\Delta} \underset{r\to\infty}{\to} e^{-|\gamma_R|r}\ e^{i|\gamma_I|r}, \qquad [3]$$

corresponding to damped, outgoing waves with a finite range, determined by the finite lifetime of the isobar.

The widths of the Δ and N^* are taken to be energy dependent according to[14]

$$\Gamma(T_{LAB}) = 2\gamma R^3\eta^3/(1 + R^2\eta^2),$$

$$\eta = \{\ \{\frac{(m+E)^2 + (m^2-\mu^2)}{2(m+E)\mu}\}^2 - (m/\mu)^2\}^{1/2},$$

$$E = 2\{[k_o^2 + m^2]^{1/2} - m\}, \qquad [4]$$

where $k_o = \{T_{LAB}m/2\}^{1/2}$ is the NN c.m. momentum, m and μ are the nucleon and pion masses; γ = 71 MeV and R = 0.81 for the Δ (Ref. 14) and γ = 110 MeV and R = 0.81 for the N^*. The channel momenta k_j^2 are computed using relativistic kinematics where

$$k_j^2 = \frac{s}{4} - \frac{1}{2}[m_j^{(1)2} + m_j^{(2)2}] + \frac{[m_j^{(1)2} - m_j^{(2)2}]^2}{4s} \qquad [5]$$

and $s = [m_1^{(1)}+m_1^{(2)}]^2 + 2m_1^{(2)}T_{LAB}$ is the invariant total energy squared. The Δ and N^* masses are assumed to be 1232 and 1440 MeV, respectively.

The core potentials are parametrized as Gaussians given by,

$$V_{core}(r) = V_o\, e^{-(r/r_o)^2}, \qquad [6]$$

based on the general forms of the NN effective local interactions calculated using the resonating group quark models of Suzuki and Hecht.[16]

The $NN(^1S_0)$, $(^3P_0)$, $(^3P_1)$, and $(^1D_2)$ phase shift and inelasticity parameters[17] from 0 - 1000 MeV have been fit using the program CALLISTO assuming the coupling schemes of Ref. 11; these being $NN(^1S_0)$ - NΔ(D), $NN(^3P_0)$ - NΔ(P) - NN^*(P), $NN(^3P_1)$ - NΔ(P), and $NN(^1D_2)$ - NΔ(S). These I = 1 channels contain the bulk of the NN inelasticity[17] and were selected for this partial survey since intermediate isobar effects at lower energies are more likely to be significant for those channels in which isobar production is greatest. Furthermore, medium modifications are most prominent in the lower NN partial waves.[4]

The symmetric core potential parameters for each case are given by the following; for $^1S_0$: V_o(NN-NN) = 10,000 MeV, V_o(NN-NΔ) = 300 MeV, V_o(NΔ-NΔ) = -200 MeV, r_o(NN-NN) = 0.3 fm, and r_o(NN-NΔ) = r_o(NΔ-NΔ) = 0.8 fm; for $^3P_0$: V_o(NN-NN) = 100,000 MeV, V_o(NN-NΔ) = V_o(NN-NN^*) = V_o(NΔ-NN^*) = 0, V_o(NΔ-NΔ) = V_o(NN^*-NN^*) = -200 MeV, r_o(NN-NN) = 5.0 fm, r_o(NΔ-NΔ) = r_o(NN^*-NN^*) = 0.8 fm; for $^3P_1$: V_o(NN-NN) = 8000 MeV, V_o(NN-NΔ) = 2000 MeV, V_o(NΔ-NΔ) = -200 MeV, and all r_o = 0.8 fm; and for $^1D_2$: V_o(NN-NN) = 5000 MeV, V_o(NN-NΔ) = 1000 MeV, V_o(NΔ-NΔ) = -200 MeV, r_o(NN-NN) = 0.6 fm, and r_o(NN-NΔ) = r_o(NΔ-NΔ) = 0.8 fm. For the $^3P_0$ channel the best results were obtained with a strong, repulsive (NN-NN) core potential and no core coupling potentials where the Δ and N^* channels are excited via the medium and long range ($r > r_c$) potentials given in Fig. 13 of Ref. 11 for the $^3P_1$ channel. The low energy phase shifts for the $^1S_0$, $^3P_0$, $^3P_1$, and $^1D_2$ channels were also fit without isobar coupling. The parameters V_o (in MeV) and r_o (in fm) for these channels are given by (10,000; 0.3), [100,000; 5.0 (effectively a hard core)], (8000; 0.8), and (5000; 0.8), respectively. The resulting fits to the WI84 phase shifts of Arndt *et al*[17] are shown in Fig. 1, where the NN elastic channel S-matrix is parametrized as $S_{\ell j} = \eta\exp(2i\delta_{\ell j})$ where $\eta = \cos^2\rho_{\ell j}$. Although the calculated $^3P_0$ phase shift is a bit too attractive, the model should provide adequate estimates of the Pauli blocking - virtual isobar correction.

The presence of intermediate isobars could alter the medium modified effective interaction as a result of the non-identity of the nucleon and isobar and because of

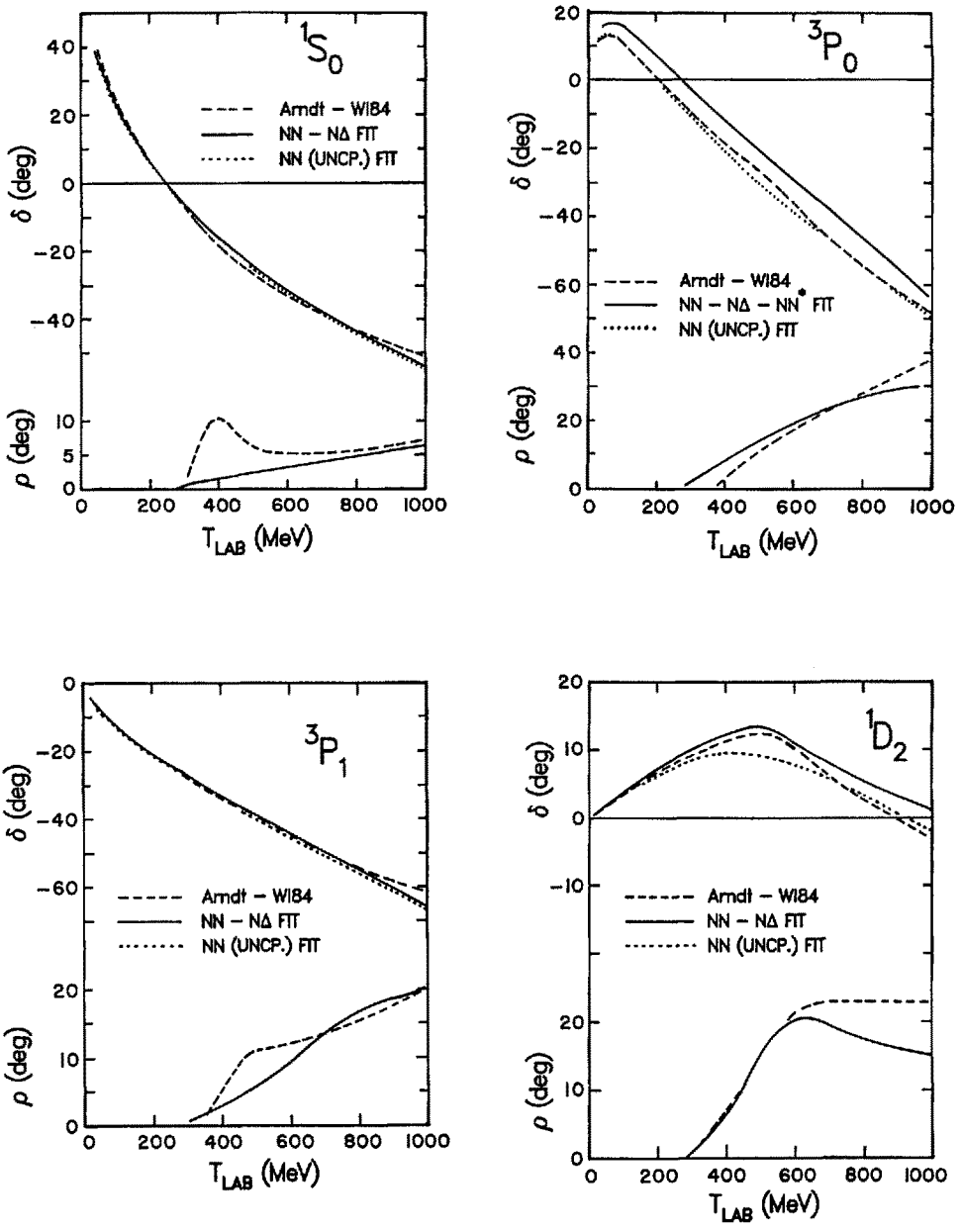

Fig. 1. Fits to the WI84 phase shifts and inelasticities of Arndt for several I = 1 NN channels using the FL + core potential model, with and without isobar coupling.

differences in the intermediate binding energy of the nucleon and isobar in the nuclear medium. Von Geramb has shown that intermediate binding energy effects are fairly small at intermediate energies; therefore only the Pauli blocking corrections will be considered here.

Pauli blocking effects have been accounted for by solving the integral equation

$$\psi = \phi + \frac{Q}{E - K + i\varepsilon} v \psi \qquad [7]$$

in coordinate space, where ψ is the correlated two-body wave function, Q is the Pauli blocking operator for an infinite nuclear medium, and v is the NN interaction. After partial wave expansions are inserted one actually solves,

$$u^{\ell'}_{\ell j}(r) = \delta_{\ell\ell'} kr\, j_\ell(kr) + 4\pi r \int_0^\infty r'dr'\, G_\ell(r,r',\omega) \times \Sigma_{\ell''} v^j_{\ell\ell''}(r')\, u^{\ell'}_{\ell'' j}(r') \qquad [8]$$

where the incident channel is denoted by ℓ' and the ℓ in $u^{\ell'}_{\ell j}(r)$ is generalized relative to the simple NN case to allow isobar channels in addition to any possible NN tensor coupled channels. $v^j_{\ell\ell''}(r)$ is the potential matrix given by

$$v^j_{\ell\ell'}(r) = \langle Y_{\ell s j}(\hat{r}) | V^j_{\ell\ell'}(\vec{r}) | Y_{\ell' s j}(\hat{r}) \rangle. \qquad [9]$$

The Greens function for NN channels is[9]

$$G_\ell(r,r',\omega) = P \int_0^\infty \frac{k'^2 dk'\, B_\ell(r,r',k')}{\omega - E(P_+) - E(P_-)} - \frac{i\pi k_o^2\, B_\ell(r,r',k_o)}{\left|\frac{d}{dk'}[E(P_+)+E(P_-)]\right|_{k'=k_o}}, \qquad [10]$$

where P denotes the principal value,

$$B_\ell(r,r',k') = \frac{1}{2\pi^2} j_\ell(k'r)\, j_\ell(k'r')\, Q_{AV}(P,k',k_F), \qquad [11]$$

Q_{AV} is the angle averaged Pauli operator (given below),[9] and

$$e \equiv \omega - E_+ - E_- = E(\vec{k}_{o1}) + E(\vec{k}_{o2}) - E(\vec{k}_1') - E(\vec{k}_2'),$$

with $\vec{k}_o$ and $\vec{k}'$ for nucleons (1) and (2) being the initial and intermediate momenta, respectively, in the reference frame of the medium. With no dispersive (binding energy) effects (e) becomes simply

$$e = \frac{\hbar^2}{2\mu}(k_o^2 - k'^2). \qquad [12]$$

For isobar channels with finite widths $G_\ell(r,r',\omega)$ is evaluated as in Eq. (10), but without the principal value and without the second, on-shell term, where k_o^2 in Eq. (12) is replaced with $\tilde{k}_j^2$ in Eq. (2). With complex isobar masses no pole (i.e., no asymptotic scattering) occurs in the propagator, hence the integral for G_ℓ may be carried out by simple quadrature.

The Pauli blocking operators are given by,

$$Q_{NN}(\vec{k}_1', \vec{k}_2') = 0 \text{ if } |\vec{k}_1'| < k_F \text{ and/or } |\vec{k}_2'| < k_F, \qquad [13a]$$

$$Q_{N\Delta}(\vec{k}_N', \vec{k}_\Delta') = 0 \text{ if } |\vec{k}_N'| < k_F \text{ , } \vec{k}_\Delta' \text{ can be anything,} \qquad [13b]$$

where k_F is the Fermi momentum and $\vec{k}_1'$, $\vec{k}_2'$, $\vec{k}_N'$ and $\vec{k}_\Delta'$ refer to intermediate momenta of the two particles in the rest frame of the medium. The angle averaged values of the above are,

$$\begin{aligned} Q_{NN} &= 0 , && \text{if } (k^2 + P^2/4) < k_F^2 \\ &= 1 , && \text{if } |k - P/2| > k_F \\ &= \frac{k^2 + P^2/4 - k_F^2}{kP} && \text{otherwise,} \end{aligned} \qquad [14a]$$

$$\begin{aligned} Q_{N\Delta} &= 0 , && \text{if } |k + P/2| < k_F \\ &= 1 , && \text{if } |P/2 - k| > k_F \\ &= \frac{1}{2}\left[1 + \frac{k^2 + P^2/4 - k_F^2}{kP}\right] && \text{otherwise,} \end{aligned} \qquad [14b]$$

and

$$Q_{\Delta\Delta} = 1, \qquad [14c]$$

where k and P are the c. m. and total momentum, respectively, of the two-body system. We assume $k_F = 1.36$ fm^{-1} in the following calculations.

The results discussed here were obtained with the coordinate space, integral equation program, ALASTOR. The model dependence of the Pauli blocking correction at low energies is examined first. Table I lists the $^1S_0$ phase shifts for several lower energies along with the changes in the phase shift and magnitude of the S-matrix, η, resulting from the above model with Pauli blocking included. These are listed for two cases; one using the Reid soft core potential;[18] the other using the Feshbach-Lomon plus Gaussian core potential given above. Isobar coupling was not included here. Stability in the Pauli blocking effects is obtained with respect to the choice of the NN interaction model.

Next, the changes in $\delta(^1S_0)$ and η resulting from Pauli blocking effects for the NN($^1S_0$) - NΔ(D) coupled channels model were calculated. These results, shown in Fig. 2 , reveal that below a few hundred MeV explicit inclusion of intermediate Δ states has very little impact on Pauli blocking effects and that above a few hundred MeV the entire Pauli correction to the $^1S_0$ channel quickly diminishes in importance. By switching on and off Pauli blocking of the intermediate Δ-isobar it is observed that the fractional change in the calculated Pauli blocking effect for $\delta(^1S_0)$ due to the distinguishability of the Δ-isobar is very small. The Pauli blocking calculations for the $^3P_0$, $^3P_1$, and $^1D_2$ channels are shown in Figs. 3-5, respectively, where results similar to that seen in the $^1S_0$ case are also found.

This work is supportive of the vast effective interaction calculations of von Geramb,[4] in which Δ degrees of freedom are not accounted for. They also suggest that medium modifications to the NR impulse approximation model for the NN effective interaction are not likely to be very significant at and above 500 MeV.

III. COMPARISON OF THE RIA WITH NR PREDICTIONS AND DATA

There are four pieces of compelling evidence which suggest that NR multiple scattering models of intermediate energy proton-nucleus scattering will be unable to account for the 500 MeV pA elastic differential cross section, A_y, and Q data.[19] The evidence includes; (1) examination of alternative density models and phase shift solutions, correlation effects, and other corrections to the NR scattering theory as discussed in Ref. 19, all of which are demonstrably inadequate to explain the differences between NR scattering predictions and the data, (2) Pauli blocking estimates above the pion production threshold, discussed in the previous section, which indicate a rapid diminution of medium effects with increasing energy, (3) comparison of the phenomenological NR effective interaction at 500 MeV (Ref. 20) with reasonable extrapolations of the von Geramb density dependent interaction; these being acutely different for the spin-orbit parts,[20] and (4) pA spin observable calculations of Dymarz[21] in which the density dependent interaction of von Geramb is extrapolated to 500 MeV, yielding poor agreement with experiment. The failure of the

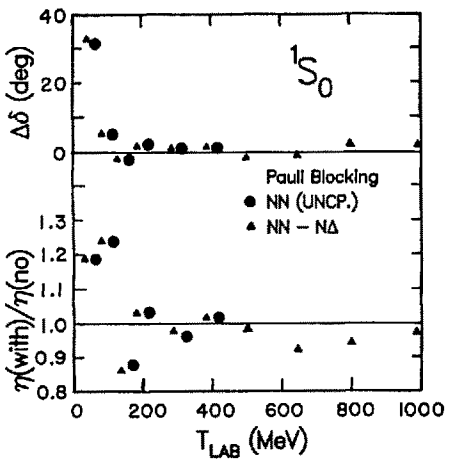

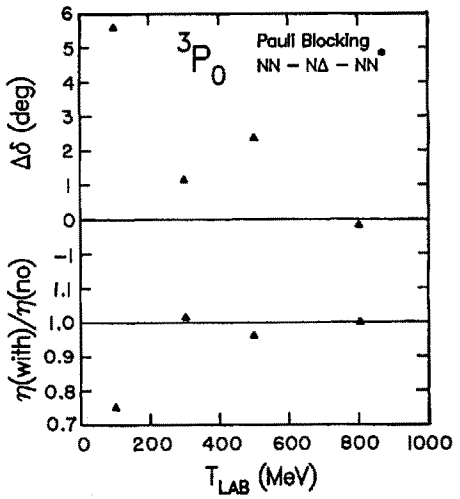

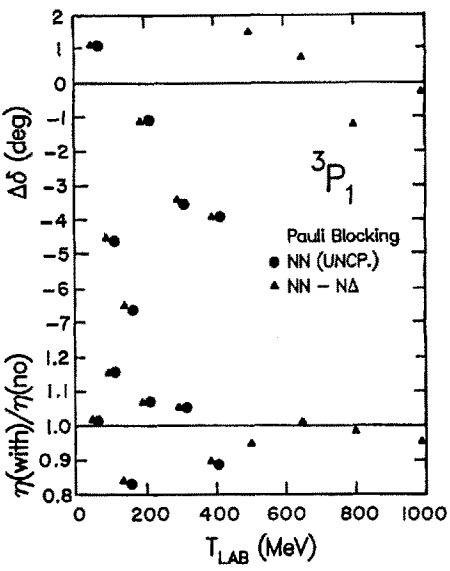

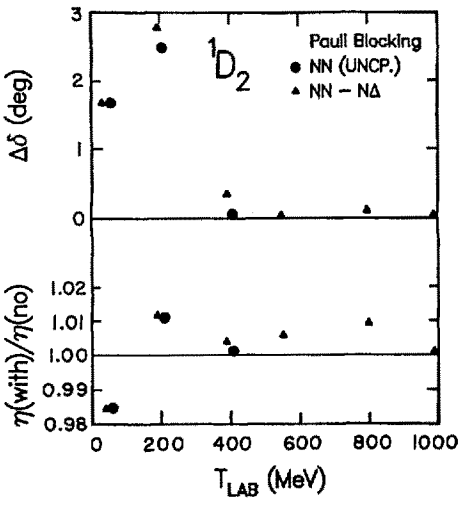

Figs. 2-5. Calculated Pauli blocking corrections to the phase shifts and magnitudes of the S-matrices for several I = 1 NN channels using the FL + core potential model, with and without isobar coupling. $\Delta\delta$ = δ(no blocking) – δ(with blocking). For E < 400 MeV the uncoupled and isobar results are offset for clarity.

TABLE I

Comparison of the Pauli Blocking Effect for $^1S_0$ using the Reid-Soft-Core and Feshbach-Lomon + Core Potentials

T_{LAB} (MeV)	$\delta(^1S_0)$ No Pauli Block	$\Delta\delta$ Reid S.C.*	η	$\Delta\delta$ FL+Core*	η
		(With Pauli Blocking)			
50	39.3	34.1	1.1996	31.6	1.1919
100	25.2	5.2	1.2485	5.3	1.2416
150	14.9	-1.5	0.8709	-1.2	0.8726
200	6.6	1.5	1.0269	1.7	1.0289
300	-6.3	0.5	0.9638	0.5	0.9689
400	-16.9	1.4	1.0135	1.4	1.0130

*Changes in phase shifts are in degrees and if positive denote reductions.

NR approaches combined with the success of the relativistic impulse approximation - Dirac equation model[5-8] suggest, very strongly, that the correct description of the proton-nucleus system demands a relativistic formulation with large and partially cancelling potentials. These strong potentials will invariably result in significant virtual pair processes.[22] The essential ingredients of the first-order RIA - Dirac equation model are given in Refs. 5-8. In this section the first-order RIA model is applied to recent data.[23]

For the calculations discussed here, the SP82 phase shift solution of Arndt[17] provided the NN amplitudes. The proton-vector densities for ^{16}O, ^{40}Ca, and ^{208}Pb were obtained by unfolding the single proton (free space) electric form factor from the nuclear charge density[24] and correcting for the neutron electric form factor and the nucleon magnetic moments.[25,26] The neutron vector density is assumed to be

$$\rho_V^n(r)|_{Theory} = \rho_V^p(r) + [\rho_n(r) - \rho_p(r)]_{HFB}, \qquad [15]$$

where HFB denotes the mean field, Hartree - Fock - Bogoliubov densities of Gogny and Dechargé.[27] The scalar densities were obtained from

$$\rho_S^{(i)}(r) = \rho_V^{(i)}(r) + [\rho_S^{(i)}(r) - \rho_V^{(i)}(r)]_{RMFT}, \qquad [16]$$

where (i) represents protons or neutrons, and the densities in the square brackets were provided by the Dirac-Hartree (relativistic) mean field (RMFT) model of Horowitz and Serot.[28]

In order to facilitate the study of the overall energy dependence of the RIA model the differential cross section data were fit by varying the neutron density while the analyzing power data were fit by varying the scalar density.[8] For the former case $\rho_V^n(r)$ was generalized to

$$\rho_V^n(r) = \rho_V^n(r)|_{Theory} + \{\frac{\rho_o'}{1 + \exp((r-c)/z)} - \frac{\rho_o}{1 + \exp((r-c_{STD})/z_{STD})}\}, \qquad [17]$$

where ρ_o and ρ_o' normalize each Woods-Saxon term, c_{STD} and z_{STD} were fixed to reproduce the surface region of $\rho_V^n(r)|_{Theory}$, and (c,z) were adjusted to minimize the $|\chi|^2$ of the fit to the data at each available energy. For this case the scalar density was fixed according to Eq. (16). Fits to the analyzing power data were accomplished by generalizing $\rho_S(r)$ to,

$$\rho_S^{(i)}(r) = \rho_V^{(i)}(r) + \xi[\rho_S^{(i)}(r) - \rho_V^{(i)}(r)]_{RMFT}, \qquad [18]$$

where ξ is varied in order to minimize $|\chi|^2$ for the A_y data, $\rho_V^n(r)$ being fixed at the theoretical value in Eq. (15).

A survey of the RIA - Dirac equation model for a wide range of energies and target masses is given in Refs. 7 and 8. Typical A_y and Q predictions of the NR-KMT impulse approximation optical potential model (NRIA)[8,25] are compared with the RIA predictions and with available data[29] in Figs. 6 and 7, respectively. Overall the RIA predictions are superior to the NRIA results. We note however an erroneous target mass dependence in the RIA model.

A summary of the energy dependence trends of the RIA model is provided in Figs. 8 - 10 which display the root-mean-square (rms) radii and the half-radius and diffuseness parameters of the vector neutron densities needed in the RIA and NRIA models to fit the available $p + {}^{40}Ca$ differential cross section data at several energies. The energy dependence and deviation from theoretical values of the deduced densities clearly demonstrate the inadequacy of both models. Notice, however, the superiority of the RIA at higher energies, whereas below 400 MeV the NRIA provides more reasonable results.

The A_y predictions are moderately sensitive to scalar-vector density differences (i.e., to the lower components of the target wave function) and the fits of the RIA model to the $p + {}^{40}Ca$ A_y data suggest a preference for $\rho_S \neq \rho_V$, at least toward the higher energies (see Fig. 10). These modest results are not meant to provide convincing evidence of target relativity. Less ambiguous and much more dramatic effects would be needed in order to demonstrate with certainty the proposed relativistic nature of bound nuclear systems.[28,30]

IV. CORRELATION CONTRIBUTIONS TO THE RIA OPTICAL POTENTIAL

Given the initial success of the standard RIA - Dirac equation approach for pA scattering the interest of theorists has subsequently turned to several related areas aimed at formally justifying and refining the model. The problems currently under consideration include; (1) attempts to provide a theoretical basis for the virtual pair dynamics based on a covariant meson exchange model of the NN interaction,[31] (2) investigation of alternative pseudo-vector coupling models for the pion-nucleon interaction[31] and for the exchange portion of the NN t-matrix,[32] (3) estimates of Pauli blocking effects on the invariant NN t-matrix,[33,34] (4) application of the RIA to (p,p′) (Ref. 35), (5) application to antiproton-nucleus[36] and meson-nucleus scattering,[37] and (6) investigation of higher order multiple scattering (correlation) effects within the standard RIA model. The latter correction will be discussed here.

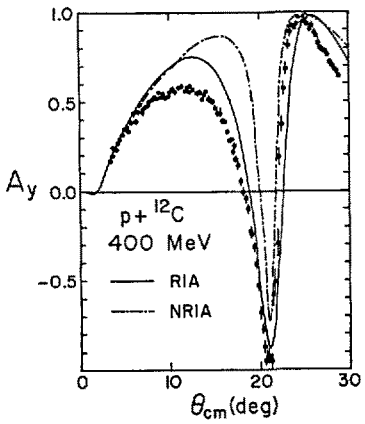

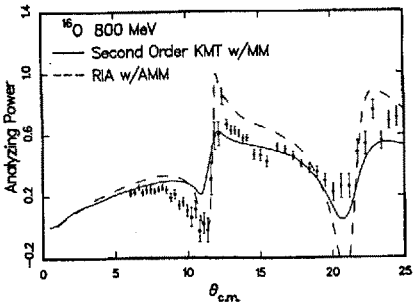

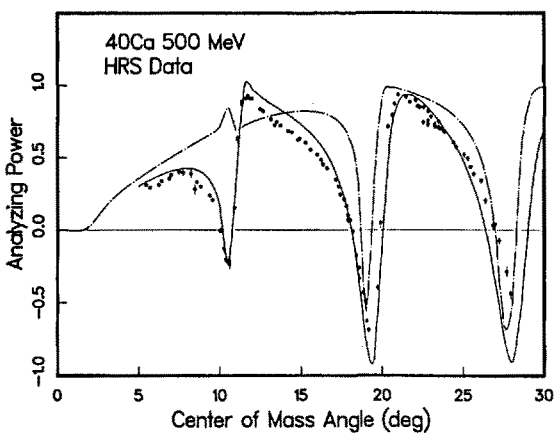

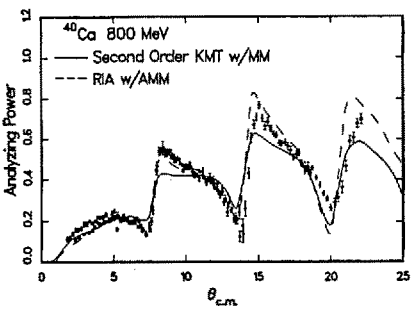

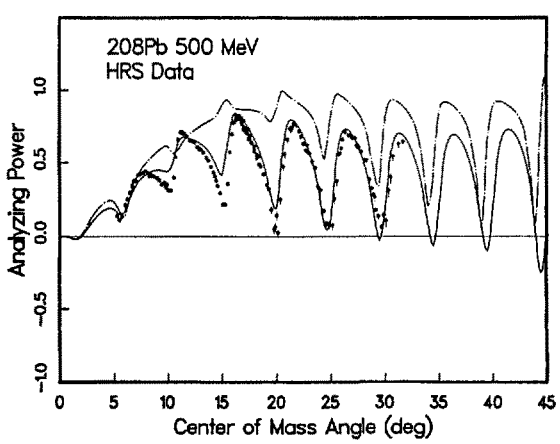

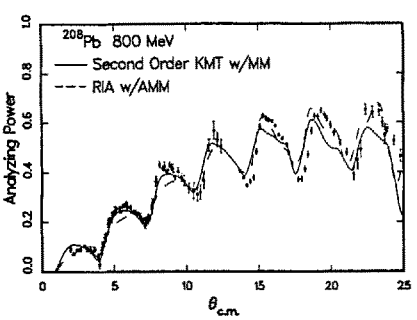

Fig. 6. Typical RIA and NRIA analyzing power predictions in comparison with available data.[29] For the cases at 400 and 500 MeV the RIA (NRIA) predictions are given by the solid (dashed-dot) curves. The p + ^{12}C 400 MeV RIA prediction was provided by B. C. Clark.

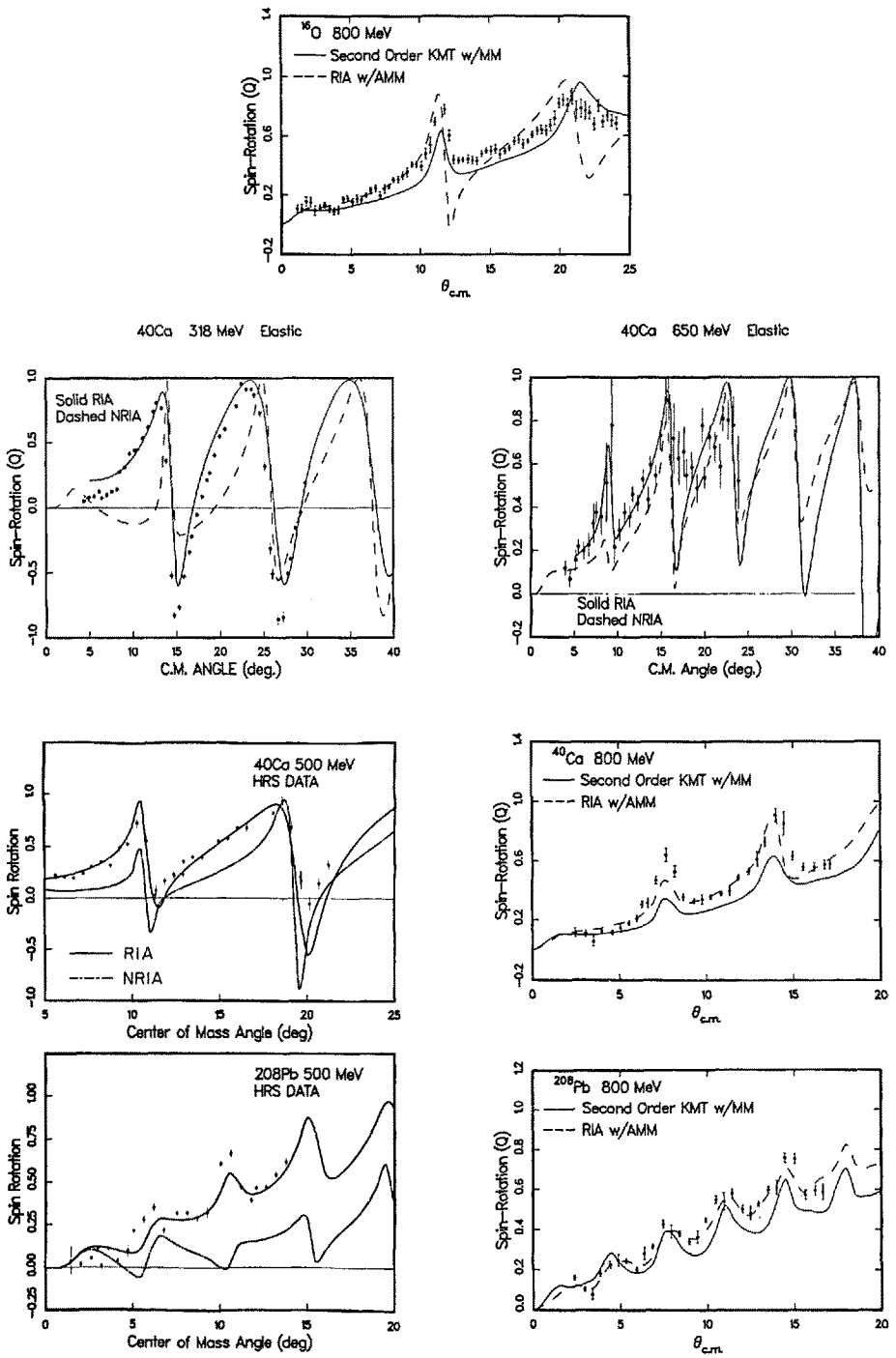

Fig. 7. Typical RIA and NRIA spin rotation predictions in comparison with data.[29]

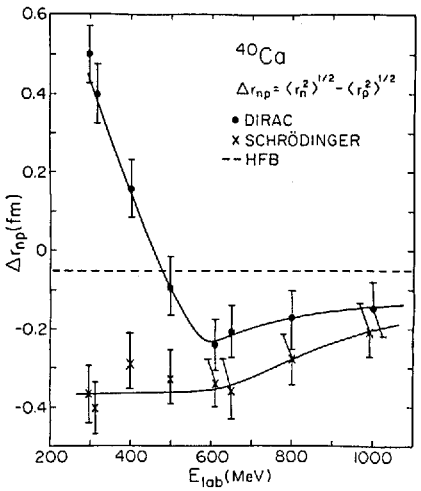

Fig. 8. Neutron-proton rms radii differences for ^{40}Ca deduced using the RIA and NRIA models as discussed in the text. The HFB theoretical value of -0.05 fm is from Ref. 27.

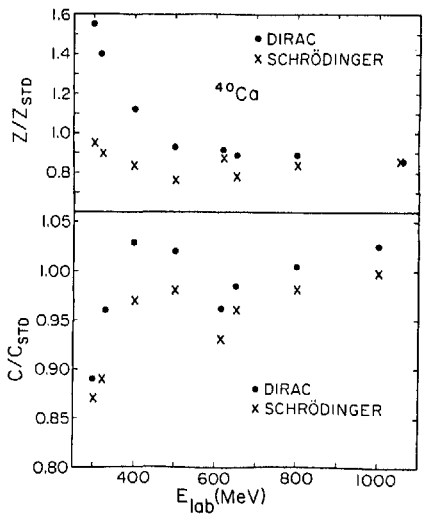

Fig. 9. Neutron geometry parameters (see Eq. (17)) needed in the RIA and NRIA models to fit the available p + ^{40}Ca differential cross section data.

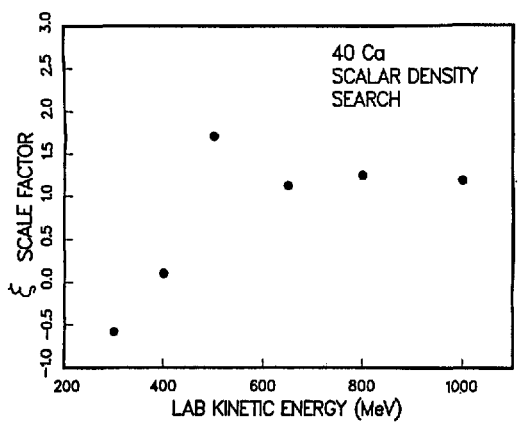

Fig. 10. Strength factor (see Eq. (18)) for the scalar-vector density difference needed to fit the p + ^{40}Ca analyzing power data.

The motivations for studying correlation effects in the RIA model are the following; (1) target nucleon correlation terms significantly affect the NRIA spin observable predictions, particularly at 800 MeV (Ref. 38); (2) the strength of the relativistic invariant NN t-matrix suggests that second order terms could be relatively larger in the RIA model than in the NR theories;[25] and (3) the convergence of the relativistic multiple scattering series needs to be investigated before committing a great deal more effort to its developement.

Expressing the second term of the relativistic optical potential in Eq. (7) of Ref. 8 in terms of sums over the individual target nucleons and using the closure approximation[39] we obtain,

$$U_{opt}^{(2)} = \sum_{i\neq j=1}^{A} \langle\tilde{\Phi}_{gs}|T_i\bar{G}T_j|\tilde{\Phi}_{gs}\rangle - \frac{(A-1)}{A}\sum_{i,j=1}^{A}\langle\tilde{\Phi}_{gs}|T_i|\tilde{\Phi}_{gs}\rangle\,\bar{G}\,\langle\tilde{\Phi}_{gs}|T_j|\tilde{\Phi}_{gs}\rangle, \qquad [19]$$

where

$$\bar{G} = (\not{p} - m - \gamma^0\bar{\varepsilon} + i\delta)^{-1} \qquad [20]$$

is an averaged Dirac propagator for the projectile; $\bar{\varepsilon}$ represents some averaged target nucleus energy eigenvalue.[8,39] The relativistic ground state target wave function is denoted by $|\tilde{\Phi}_{gs}\rangle$ (see Ref. 8) and the invariant NN t-matrix, defined in Ref. 8, for the i^{th} target nucleon is represented by T_i. The T_i are kinematically related to the invariant NN scattering amplitudes $\hat{F}$ (see Appendix B of Ref. 8); the latter are assumed to be represented by[40]

$$\hat{F} = F_S I_1 I_2 + F_P \gamma_1^5\gamma_2^5 + F_V \gamma_1^\mu\gamma_{2\mu} + F_A\gamma_1^5\gamma_1^\mu\gamma_2^5\gamma_{2\mu} + F_T\sigma_1^{\mu\nu}\sigma_{2\mu\nu} \equiv \sum_\beta \hat{F}_\beta\, O_{1\beta}\, O_{2\beta}\,. \qquad [21]$$

The invariant amplitudes are determined from positive energy, NN scattering data.[40]

Explicit evaluation of Eq. (19) in momentum space, assuming local interactions and the expansion for $T_i(q)$ in Eq. (21), yields

$$U_{opt}^{(2)}(\vec{k},\vec{k}') = (2\pi)^{-3}\sum_{\gamma,\delta=S,P,V,A,T}\;\sum_{\alpha,\beta=occ}\iiint d^3r_1 d^3r_2 d^3k''\; e^{i(\vec{k}''-\vec{k}')\cdot\vec{r}_1}\, e^{i(\vec{k}-\vec{k}'')\cdot\vec{r}_2} \times[T_\gamma(\vec{k}''-\vec{k}')O_{1\gamma}\bar{G}(\vec{k}'')O_{1\delta}T_\delta(\vec{k}-\vec{k}'')] \times[\tfrac{1}{A}B^\gamma_{\alpha\alpha}(\vec{r}_1)B^\delta_{\beta\beta}(\vec{r}_2) - B^\gamma_{\alpha\beta}(\vec{r}_1)B^\delta_{\beta\alpha}(\vec{r}_2)] \qquad [22]$$

where the first two summations correspond to those in Eq. (21), the second pair of summations includes all occupied orbitals. The quantities in the first set of brackets involve the projectile operators, scattering amplitudes, and Dirac propagator, whereas those in the second set of brackets contain nuclear structure (correlation) information. The B's in Eq. (22) are defined according to,

$$B^{\gamma}_{\alpha\beta}(\vec{r}) \equiv \bar{\zeta}_{\alpha}(\vec{r})\, O_{2\gamma}\, \zeta_{\beta}(\vec{r}), \qquad [23]$$

where $\zeta_{\alpha}(\vec{r})$ are the relativistic, four-component single nucleon wave functions.[8,28] The explicit momentum space representation of the Dirac projectile propagator is given by (the $\bar{\epsilon}$ in Eq. (20) is ignored)

$$\bar{G}(\vec{k}'') = \frac{(E_{k''}\gamma_1^0 - \vec{\gamma}_1\cdot\vec{k}'' + m)}{2E_{k''}}\left[P\left\{\frac{1}{E-E_{k''}}\right\} - i\pi\delta(E-E_{k''})\right]$$

$$+ \frac{E_{k''}\gamma_1^0 + \vec{\gamma}_1\cdot\vec{k}'' - m}{2E_{k''}(E+E_{k''})} \qquad [24]$$

where $E_{k''} = \sqrt{k''^2 + m^2}$ and P denotes the Cauchy principal value. The three terms in $\bar{G}(\vec{k}'')$ correspond to propagation of positive energy off-shell, on-shell, and negative energy intermediate states, respectively.

In principle the non-local, second order RIA optical potential in Eq. (22) could be evaluated. However, for this preliminary estimate Eq. (22) can be greatly simplified by making two, very reasonable simplifications. These are the following; (1) ignore the lower components of the target wave function, thus restricting the contributing parts of the NN interaction to scalar, time-like vector, space-like axial vector, and space-like tensor terms and (2) ignore these latter two terms in the NN interaction since both are very small relative to T_S and T_V.[40] With these assumptions the NN t-matrix operators act on the target wave function as if they were scalars, hence the NN operators and target wave functions can be commuted and $U^{(2)}_{opt}$ written as,

$$U^{(2)}_{opt}(\vec{k},\vec{k}') = \frac{A(A-1)}{(2\pi)^3}\sum_{\gamma,\delta=S,V}\int d^3k''\, T_{\gamma}(\vec{k}''-\vec{k}')\, O_{1\gamma}\bar{G}(\vec{k}'')\, O_{1\delta}\, T_{\delta}(\vec{k}-\vec{k}'')$$

$$\times\tilde{C}_{(2)}(\vec{k}''-\vec{k}',\vec{k}-\vec{k}''), \qquad [25]$$

where $\tilde{C}_{(2)}$ is the usual two-body correlation function form factor appearing in NR optical potentials.[3,25,39,41]

For this initial estimate only on-shell intermediate propagation will be included. The E > 0 off-shell portion of $\bar{G}$ is not likely to be very important based on studies of the analogous contribution to the NR optical potential. The negative energy propagation could be important and is currently being evaluated.[42] The non-locality in $U^{(2)}_{opt}$ associated with the $\vec{\gamma}_1 \cdot \vec{k}''$ term in $\bar{G}(\vec{k}'')$ will be included; however the other sources of non-locality which are common to NRIA second order optical potentials will be ignored based on experience with these NR calculations.[25,39,41] Defining the momentum transfers $\vec{q} = \vec{k} - \vec{k}'$ and $\vec{q}'' = \vec{k}'' - \vec{k}_a$ where $\vec{k}_a = (\vec{k} + \vec{k}')/2$, the second order RIA optical potential becomes

$$U^{(2)}_{opt} = -\frac{i\pi}{2K_E\hbar c}\frac{A(A-1)}{(2\pi)^3}\sum_{\gamma,\delta=S,V}\int d^2q''\, T_\gamma(\frac{\vec{q}}{2}+\vec{q}'')\, O_{1\gamma}$$

$$\times[\gamma^o_1 E - \vec{\gamma}\cdot\vec{q}'' + m + \frac{i}{2}\vec{\gamma}_1\cdot\vec{\nabla}_r|_U + i\vec{\gamma}_1\cdot\vec{\nabla}_r|_{WF}]$$

$$\times O_{1\delta}\, T_\delta(\frac{\vec{q}}{2}-\vec{q}'')\, \tilde{C}_{(2)}(\frac{\vec{q}}{2}+\vec{q}'', \frac{\vec{q}}{2}-\vec{q}''), \qquad [26]$$

where $K_E = \sqrt{E^2 - m^2c^4}$ (in MeV) and $\vec{\nabla}_r|_U$ ($\vec{\nabla}_r|_{WF}$) acts on coordinate (r) for the local portion of the optical potential (wave function). The two-dimensional integration in Eq. (26) can be handled analytically if it is further assumed that; (1) the relevant momentum transfers $q << K_E/(\hbar c)$, (2) the correlation function can be expressed as

$$C_{(2)}(\vec{r}_1,\vec{r}_2) = f(|\vec{r}_1 - \vec{r}_2|)\rho_1(\vec{r}_1)\rho_1(\vec{r}_2), \qquad [27]$$

(3) f(x) and T can be approximated with Gaussian forms, and (4) the ranges of f(x) and T(r) are small compared to the nuclear size. Each of these latter four approximations are common to NRIA models and are quite reasonable.[25,39,41] Under these assumptions the local, second order RIA optical potential in coordinate space becomes,

$$U^{(2)}_{opt}(r) = U^{(2)}_S 1_1 + U^{(2)}_V \gamma^o_1 + iU^{(2)}_r \vec{\gamma}\cdot\hat{r} + U'^{(2)}\vec{\gamma}\cdot\vec{p} \qquad [28a]$$

where

$$U_S^{(2)} = m(U_{SS} + U_{VV}) + 2EU_{SV},$$

$$U_V^{(2)} = E(U_{SS} + U_{VV}) + 2mU_{SV},$$

$$U_r^{(2)} = \frac{\hbar c}{2}\frac{d}{dr}(U_{SS} - U_{VV}),$$

$$U'^{(2)} = U_{VV} - U_{SS}, \qquad [28b]$$

and

$$U_{\gamma\delta}(r) = \frac{-i\pi A(A-1)}{2K_E\hbar c(2\pi)^6} S_{\gamma\delta}(0)\int d^3q e^{-i\vec{q}\cdot\vec{r}} T_\gamma(q/2)\ T_\delta(q/2)\ \tilde{\rho}^2_{\gamma\delta}(q), \qquad [28c]$$

where γ and δ represent scalar and vector and

$$\tilde{\rho}^2_{\gamma\delta}(q) = \int d^3r e^{i\vec{q}\cdot\vec{r}}\rho_1{}^2(\vec{r})S_{\gamma\delta}(r)/S_{\gamma\delta}(0). \qquad [28d]$$

$\rho_1(\vec{r})$ is the one-body matter density normalized such that $\int d^3r\rho_1(r) = 1$. The correlation range factor S is given by,

$$S_{\gamma\delta}(r) = \sum_{\alpha=1}^{3} \frac{\pi^{5/2}R_\alpha f_\alpha}{(B_\gamma + B_\delta)}\left[\frac{1}{4(B_\gamma + B_\delta)} + R_\alpha^{-2}\right]^{-1}. \qquad [28e]$$

In the above equation the sum accounts for contributions from Pauli, short-range repulsion and Pauli-short-range interference correlations[25,39] where the function f(x) is written as[39]

$$f(x) = \sum_{\alpha=1}^{3} f_\alpha e^{-x^2/R_\alpha{}^2}. \qquad [29]$$

The values of f_α and R_α are given in Ref. 25. Since the Pauli correlation depends on the local Fermi momentum, the R_α are density dependent causing the correlation range factor to depend on r. The B_γ appear in the expression for S in order to correct for the finite range of the NN interaction where it is assumed that

$$T_\gamma(q) = T_\gamma(0)e^{-B_\gamma q^2}. \qquad [30]$$

For the SP82 NN scattering amplitudes B_S and B_V are 0.18 fm^2 and 0.15 fm^2 at 300 MeV, 0.15 fm^2 and 0.12 fm^2 at 500 MeV, and 0.14 fm^2 and 0.12 fm^2 at 800 MeV, respectively.

This Gaussian form is used only in calculating $S_{\gamma\delta}(r)$ and not for the $T(q/2)$ in Eq. (28c) or in the first-order potential.[8]

The Dirac equation with the first order RIA optical potential plus the above non-local, second order RIA optical potential, given by

$$[\vec{\alpha}_1\cdot\vec{p} + \beta_1(m + U_{opt}^{(1)} + U_{opt}^{(2)}) - E]\begin{pmatrix}\phi_U\\ \phi_L\end{pmatrix} = 0, \qquad [31]$$

is solved for the upper two-component wave function ϕ_U, by formally eliminating the dependence on the lower component. The resulting second order differential equation can be transformed into Schrödinger equation form as discussed in Ref. 43 and in the contribution of Prof. B. C. Clark to these conference proceedings. The discussion in Ref. 43 accounts for local, relativistic optical potentials with scalar, time and space-like vector, and tensor components. The non-locality contribution, $U'^{(2)}\vec{\gamma}\cdot\vec{p}$, in Eq. (28a) is included by combining this term with the $\vec{\alpha}_1\cdot\vec{p}$ portion of the projectile Hamiltonian. This leads to a new transformation for the upper component wave function, given by

$$\phi_U(\vec{r}) = K(r)\phi(\vec{r}) \qquad [32a]$$

$$K(r) = \sqrt{A_2(r)}\,\exp[\int drF(r)/(2\hbar)], \qquad [32b]$$

$$A_2(r) = \frac{E + m + U_S(r) - U_V(r)}{(E + m)[1 + U'^{(2)}(r)]}\ , \qquad [32c]$$

and

$$F(r) = \frac{2U_r^{(2)}(r)}{1 + U'^{(2)}(r)}\ . \qquad [32d]$$

Employing the wave function transformation in Eq. (32a) leads to a Schrödinger-like second order differential equation for $\phi(\vec{r})$ with local, effective central and spin-orbit optical potentials. These latter terms are explicitly dependent on the non-local relativistic potential $U'^{(2)}(r)$. Since $\phi(\vec{r}) \to \phi_U(\vec{r})$ at infinity, the asymptotic portion of $\phi_U(\vec{r})$ and the resulting phase shifts, scattering amplitudes, and elastic observables are readily obtained.[44]

RIA calculations were carried out for p + ^{16}O, ^{40}Ca, and ^{208}Pb at 300, 500, 800 MeV where the standard first-order RIA predictions (as discussed in Ref. 8) are compared to RIA calculations with $U_{opt}^{(2)}$ included. Some typical results are shown in Figs. 11-13 for the elastic differential cross sections, A_y and Q, respectively. The effects on the differential cross section are similar to that seen in NRIA

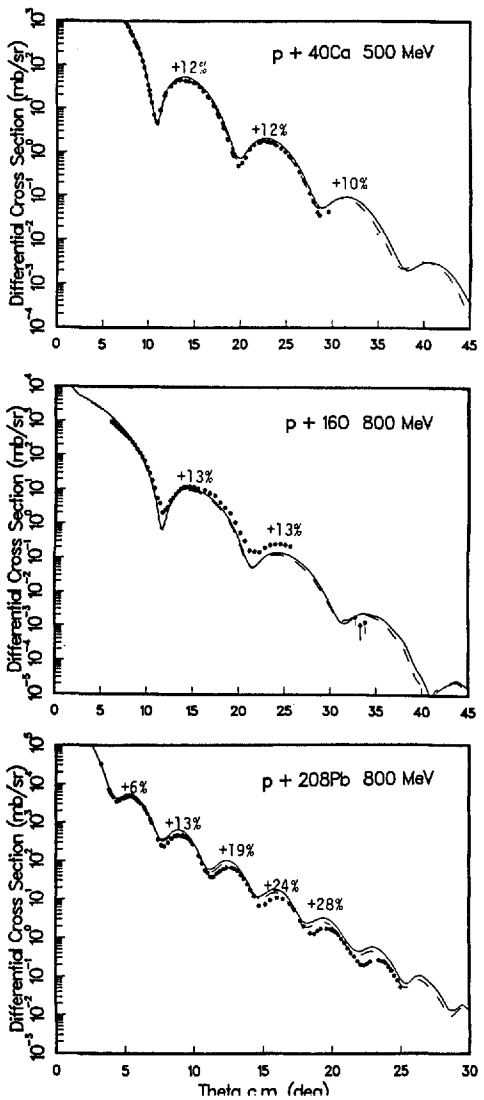

Fig. 11. Typical changes in the RIA elastic differential cross section predictions due to correlation effects as discussed in the text. RIA calculations with (without) correlations are denoted by the solid (dashed) curves. The numbers indicate the percent increases at each diffractive maximum.

calculations[25,39] where moderate (5 - 30%) increases in the predicted overall magnitudes of the angular distributions are noted (see Fig. 11). However, unlike the NR correlation contributions, the spin observables are scarcely affected at all by the relativistic correlation terms, at least as estimated here. This is both good and bad, since the excellent predictions for A_y and Q obtained with the first-order RIA are not ruined, but, on the other hand, the inferior RIA predictions for light targets and the incorrect RIA mass dependence (see previous section) are not alleviated.

The diminutive size of these correlation effects can be qualitatively understood. The scalar and vector terms are the dominant parts of $U_{opt}^{(2)}$ in Eq. (28a). In the limit of zero-range NN interactions $U_{\gamma\delta}(r)$ in Eq. (28c) has the form

$$U_{\gamma\delta}(r) \simeq T_\gamma(0)T_\delta(0)C\rho^2(r) \qquad [33]$$

where C absorbs the kinematic factors and correlation length parameter in Eq. (28c). Therefore at lower energies ($E \simeq m$) $U_{opt}^{(2)}$ is roughly,

$$\begin{aligned} U_{opt}^{(2)}(r) &\simeq (T_S(0) + T_V(0)\gamma^o)(1 + \gamma^o)(T_S(0) + T_V(0)\gamma^o)E\ C\rho^2(r) \\ &\simeq (T_S(0)^2 + 2T_S(0)T_V(0) + T_V(0)^2)(1 + \gamma^o)E\ C\rho^2(r) \\ &\simeq (T_S(0) + T_V(0))^2(1 + \gamma^o)E\ C\rho^2(r). \end{aligned} \qquad [34]$$

Each individual term in Eq. (34) (or in Eq. (28b)) is fairly large, being 5-30% of $U_{opt}^{(1)}$ in order-of-magnitude. From Eq. (34) it is seen however that the second order scalar and vector potentials are proportional to $(T_S(0) + T_V(0))^2$, hence cancellations occur between the scalar and vector amplitudes,[40] thus suppressing the contributions of $U_S^{(2)}$ and $U_V^{(2)}$. In the same manner it is noted that the virtual pair contribution to $U_{opt}^{(2)}$ (propagator proportional to $E\gamma^o - m$, see Eq. (24)) depends on $(T_S(0) - T_V(0))^2$ so that constructive additions occur; hence these contributions to $U_{opt}^{(2)}$ might be of greater significance. These latter contributions along with those which arise from treating the target wave function relativistically (which will then allow contributions of the very large pseudo-scalar NN interaction) are the subject of current research and will be reported on later.[42]

V. CONCLUSIONS AND PROSPECTUS

Concerning the effects of Pauli blocking in intermediate NN states in NR effective interactions it has been shown that the neglect of virtual isobars by

Jeukenne, Lejeune, and Mahaux,[9] Brieva and Rook[10] and von Geramb[4] is justifiable for NN energies below pion production threshold. The partial survey of NN, I = 1 partial wave channels conducted here suggests that Pauli blocking effects rapidly diminish with increasing projectile energies above 400 MeV. Completion of the Pauli blocking calculations using the coupled channels isobar model discussed here as well as other, recent NN interaction models above 350 MeV should be carried out in the near future and will finally determine whether or not nonrelativistic scattering models are capable of explaining the 500-1000 MeV proton-nucleus elastic scattering data. Theoretical developement of NR calculations should by no means be abandoned so long as this important question remains without a definitive answer.

Several new applications of the standard relativistic impulse approximation - Dirac equation model to recent 800 MeV pA spin observable data[23] have been shown. These further exemplify the facility of the RIA model in accounting for intermediate energy proton-nucleus spin measurements. Further indication of the erroneous target mass dependence of the first-order RIA model is also to be seen in the results of section III.

Concerning the estimates of correlation effects it was found that the individual second order optical potential terms are fairly large relative to the first-order RIA potential as expected, however cancellations among the various second order terms result in a very small correlation contribution to the overall proton-nucleus scattering matrix. Improved calculations with virtual pair and off-shell processes as well as with lower component target wave functions may lead to more sizeable effects.

A better understanding of the projectile virtual pair process along with relativistic medium modifications and a theoretical basis for a relativistic multiple scattering theory should form the cornerstone of research aimed at fully developing an accurate, covariant theory of the nucleon-nucleus system. It appears at this time that the nucleon-nucleus system will eventually be successfully understood in terms of some sort of relativistic approach. However, more work in both the NR and relativistic frameworks is needed before final conclusions can be drawn.

Many enlightening conversations with Profs. G. W. Hoffmann, B. C. Clark, E. L. Lomon and H. V. von Geramb as well as the support of the U. S. Department of Energy and The Robert A. Welch Foundation are gratefully acknowledged.

REFERENCES

1. K. A. Brueckner and C. A. Levinson, Phys. Rev. 97 (1955) 1344.
2. K. M. Watson, Phys. Rev. 89 (1953) 575.
3. A. K. Kerman, H. McManus and R. M. Thaler, Ann. Phys. (N. Y.) 8 (1959) 551.
4. H. V. von Geramb, in The Interaction Between Medium Energy Nucleons in Nuclei - 1982, American Institute of Physics Conf. Proc. No. 97, edited by H. O. Meyer (American Institute of Physics Press, New York, 1983), p.44; and L. Rikus and H.

V. von Geramb, Nucl. Phys. A426 (1984) 496, and H. V. von Geramb, private communication.
5. J. A. McNeil, J. Shepard, and S. J. Wallace, Phys. Rev. Lett. 50 (1983) 1439,1443.
6. B. C. Clark, S. Hama, R. L. Mercer, L. Ray and B. D. Serot, Phys. Rev. Lett. 50 (1983) 1644.
7. B. C. Clark, S. Hama, R. L. Mercer, L. Ray, G. W. Hoffmann, and B. D. Serot, Phys. Rev. C28 (1983) 1421.
8. L. Ray and G. W. Hoffmann, Phys. Rev. C31 (1985) 538.
9. J.-P. Jeukenne, A. Lejeune and C. Mahaux, Phys. Rev. C10 (1974) 1391.
10. F. A. Brieva and J. R. Rook, Nucl. Phys. A291 (1977) 299,317.
11. E. L. Lomon, Phys. Rev. D26 (1982) 576.
12. T.-S. H. Lee, Phys. Rev. C29 (1984) 195.
13. J. H. Gruben and B. J. VerWest, Phys. Rev. C28 (1983) 836.
14. A. M. Green, J. A. Niskanen and M. E. Sainio, J. Phys. G: Nucl. Phys. 4 (1978) 1055.
15. E. L. Lomon and H. Feshbach, Ann. Phys. (N. Y.) 48 (1968) 94.
16. Y. Suzuki and K. T. Hecht, Phys. Rev. C27 (1983) 299.
17. R. A. Arndt et al., Phys. Rev. D28 (1983) 97 and R. A. Arndt, private communication. Both the SP82 and WI84 phase shift solutions were obtained from the V.P.I. scattering analysis interactive dial-in computer program (SAID).
18. R. V. Reid, Ann. Phys. (N. Y.) 50 (1968) 411.
19. G. W. Hoffmann et al., Phys. Rev. Lett. 47 (1981) 1436.
20. M. L. Barlett, W. R. Coker, G. W. Hoffmann, and L. Ray, Phys. Rev. C29 (1984) 1407.
21. R. Dymarz, Phys. Lett. 152B (1985) 319.
22. M. V. Hynes, A. Picklesimer, P. C. Tandy and R. M. Thaler, Phys. Rev. C31 (1985) 1438, and ibid. Phys. Rev. Lett. 52 (1984) 978.
23. R. W. Fergerson et al., submitted to Phys. Rev. C (1985).
24. I. Sick and J. S. McCarthy, Nucl. Phys. A150 (1970) 631; I. Sick et al., Phys. Lett. 88B (1979) 245; and B. Frois et al., Phys. Rev. Lett. 38 (1977) 152.
25. L. Ray, Phys. Rev. C19 (1979) 1855.
26. W. Bertozzi, J. Friar, J. Heisenberg, and J. W. Negele, Phys. Lett. 41B (1972) 408.
27. J. Dechargé and D. Gogny, Phys. Rev. C21 (1980) 1568; J. Dechargé, M. Girod, D. Gogny, and B. Grammaticos, Nucl. Phys. A358 (1981) 203c; J. Dechargé, private communication.
28. C. J. Horowitz and B. D. Serot, Nucl. Phys. A368 (1981) 503.
29. The 500 MeV Los Alamos Meson Physics Facility - high resolution spectrometer (LAMPF-HRS) data are published in Ref. 19. The 800 MeV ^{40}Ca HRS analyzing power data are presented in G. Igo et al., Phys. Lett. 81B (1979) 151. The 800 MeV ^{208}Pb HRS cross section data appear in G. W. Hoffmann et al., Phys. Rev. C21 (1980) 1488 and the analyzing power data are given in Ref. 38. The 500 MeV p + ^{40}Ca HRS spin rotation data are from A. Rahbar et al., Phys. Rev. Lett. 47 (1981) 1811 while the 500 MeV ^{208}Pb Q data are from B. Aas et al., Bull. Am. Phys. Soc. 26 (1981) 1125; and B. Aas (private communication). The 800 MeV p + ^{16}O cross section and analyzing power data are from G. S. Adams et al., Phys. Rev. Lett. 43 (1979) 421. The 800 MeV Q data are from Ref. 23 while the p + ^{40}Ca, 318 and 650 MeV Q data are from B. Aas, priv. comm. The 400 MeV p + ^{12}C A_y data are from K. W. Jones et al., Ph. D. thesis, Rutgers University and Los Alamos National Laboratory, Los Alamos preprint LA-10064-T (unpublished) and K. W. Jones et al., to be submitted to Phys. Rev. C (1985).
30. B. D. Serot and J. D. Walecka, to be published in Advances in Nuclear Physics, edited by J. W. Negele and E. Vogt (Plenum, New York).
31. J. A. Tjon and S. J. Wallace, Univ. of Maryland preprints #85-052 and ORO 5126-244 (1985) unpublished.
32. C. J. Horowitz, Phys. Rev. C31 (1985) 1340.
33. C. J. Horowitz, in the proceedings of the LAMPF workshop on "Dirac Approaches to Nuclear Physics," Los Alamos National Laboratory Conference Report, Los Alamos, N.M. (1985), unpublished.
34. M. R. Anastasio, L. S. Celenza, W. S. Pong and C. M. Shakin, Phys. Rep. 100 (1983) 327.

35. J. R. Shepard, E. Rost, and J. Piekarewicz, Phys. Rev. C30 (1984) 1604; E. Rost, J. R. Shepard, E. R. Siciliano and J. A. McNeil, Phys. Rev. C29 (1984) 209; and D. A. Sparrow et al., Phys. Rev. Lett. 54 (1985) 2207.
36. B. C. Clark et al., Phys. Rev. Lett. 53 (1984) 1423 and A. Picklesimer, P. C. Tandy and J. A. Tjon, unpublished.
37. B. C. Clark, S. Hama, G. R. Kälbermann, R. L. Mercer and L. Ray, submitted to Phys. Rev. Lett. (1985).
38. G. W. Hoffmann et al., Phys. Rev. C24 (1981) 541.
39. H. Feshbach, A. Gal, and J. Hüfner, Ann. Phys. (N. Y.) 66 (1971) 20; and E. Boridy and H. Feshbach, Ann. Phys. (N. Y.) 109 (1977) 468.
40. J. A. McNeil, L. Ray and S. J. Wallace, Phys. Rev. C27 (1983) 2123.
41. A. Chaumeaux, V. Layly and R. Schaeffer, Ann. Phys. (N. Y.) 116 (1978) 247.
42. J. D. Lumpe and L. Ray, unpublished.
43. B. C. Clark, S. Hama, and R. L. Mercer, in The Interaction Between Medium Energy Nucleons in Nuclei - 1982, American Institute of Physics Conf. Proc. No. 97, edited by H. O. Meyer (American Institute of Physics Press, New York, 1983), p.260.
44. E. D. Cooper, Ph. D. thesis, University of Alberta, 1981 (unpublished).

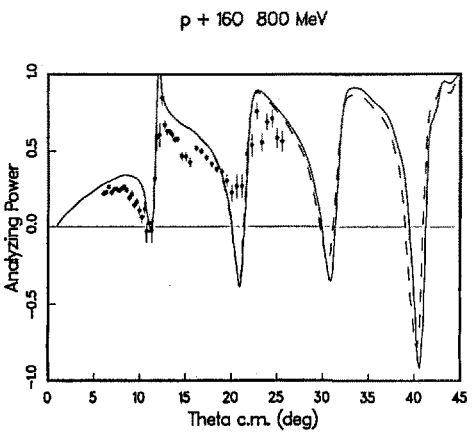

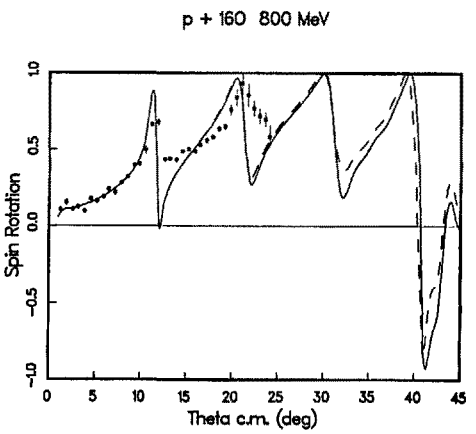

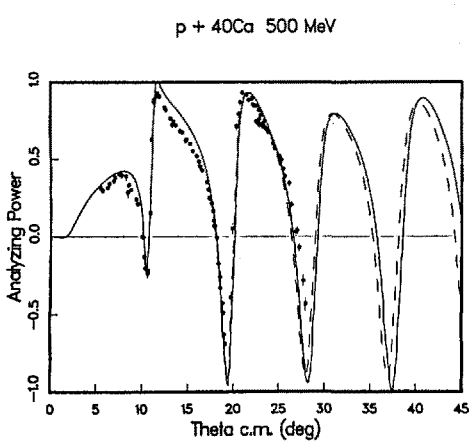

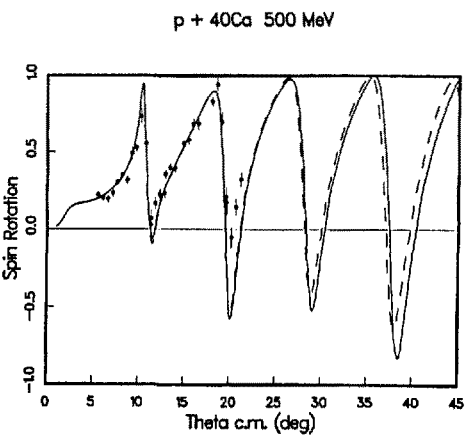

Fig. 12. Same as Fig. 11, except for analyzing powers.

Fig. 13. Same as Fig. 11, except for spin rotations.